International Geology Review

ISSN: 0020-6814 (Print) 1938-2839 (Online) Journal homepage: http://www.tandfonline.com/loi/tigr20

Intraplate extension of the Indochina plate deduced from 26 to 24 Ma A-type granites and tectonic implications

Xinyu Wang, Xin Yao, Shifeng Wang, Xinyou Zhu, Jingbin Wang & Chao Wang

To cite this article: Xinyu Wang, Xin Yao, Shifeng Wang, Xinyou Zhu, Jingbin Wang & Chao Wang (2018): Intraplate extension of the Indochina plate deduced from 26 to 24 Ma A-type granites and tectonic implications, International Geology Review, DOI: 10.1080/00206814.2018.1531356

To link to this article: https://doi.org/10.1080/00206814.2018.1531356

View supplementary material

Published online: 11 Oct 2018.

Submit your article to this journal

View Crossmark data

Full Terms & Conditions of access and use can be found at
http://www.tandfonline.com/action/journalInformation?journalCode=tigr20

INTERNATIONAL GEOLOGY REVIEW
https://doi.org/10.1080/00206814.2018.1531356

Taylor & Francis
Taylor & Francis Group

ARTICLE

Check for updates

Intraplate extension of the Indochina plate deduced from 26 to 24 Ma A-type granites and tectonic implications

Xinyu Wang[a,b], Xin Yao[a], Shifeng Wang[a], Xinyou Zhu[b], Jingbin Wang[b] and Chao Wang[c]

[a]Key laboratory of Neotectonic Movement and GeoHazard, Ministry of Land and Resources, Institute of Geomechanics, Chinese Academy of Geological Sciences, Beijing, China; [b]Beijing Institute of Geology for Mineral Resources, Beijing, China; [c]Institute of Tibetan Plateau Research, Chinese Academy of Sciences, Beijing, China

ABSTRACT
In recent years, abundant Cenozoic potassic magmatic rocks from eastern Tibet and the Indochina Block have been studied extensively; however, until now, knowledge of Cenozoic A-type granites from the interior of the Indochina Block has been limited. U–Pb zircon ages for six samples of the Salei granite pluton within the Indochina Block range from 26 to 24 Ma. *In situ* Lu–Hf and Sr–Nd isotope data indicate that the Salei pluton was sourced mostly from Mesoproterozoic basement rocks of the Indochina Block, mixed with a small volume of juvenile crust derived from the underplated mantle. Whole-rock major element geochemistry indicates that the six samples are peraluminous high-K calc-alkaline granites. The trace and rare earth element patterns are typical of within-plate A-type granites. In combination with previous research, the present results suggest that the late Oligocene Salei granite formed from the convective removal of thickened lower continental lithospheric mantle. Moreover, the presence of 26–24 Ma A-type granites in the Indochina Block indicates within-plate extension in the interior of the block during the late Oligocene.

ARTICLE HISTORY
Received 3 January 2018
Accepted 30 September 2018

KEYWORDS
Indochina block; A-type granite; U–Pb zircon age; geochemistry; Sr–Nd–Hf isotopes; intraplate extension; Cenozoic

1. Introduction

Cenozoic (ca. 50–0 Ma) potassic to ultrapotassic mafic volcanic and potassic felsic intrusive magmatic suites are common throughout the eastern Indo-Asia collision zone. This zone extends for over 2000 km along the Jinshajiang–Ailaoshan–Red River tectonic belt and across eastern Tibet, the Lanping–Simao area, and the Indochina block (Chung *et al*. 1998; Deng *et al*. 2014). This region is characterized by high topographic relief and is bounded by a series of north- and northwest-striking Cenozoic faults: to the west by the Gaoligong and Batang–Lijiang strike-slip systems; to the east by the Longmen Shan Thrust Belt and the Xiaojiang Fault; and to the south by the Red River Fault (Wang *et al*. 1997; Figure 1). South of the Red River Fault, the Indochina Block is strongly deformed in the north but behaves more like a rigid block in the south. In eastern Tibet, both Cenozoic igneous rocks and a series of early-middle Cenozoic basins are located along a 100 km-wide narrow belt following the Nangqian Thrust Belt, the Batang-Lijiang fault system, and the Red River shear zone (Figure 1). In contrast, Cenozoic igneous rocks are widespread distributed in the 500-km-wide Indochina block (Figure 1).

In recent years, these Cenozoic potassic magmatic rocks have been studied extensively, and their geochronology, petrogenesis and tectonic evolution are debated. These rocks become progressively younger from north to south (Figure 1; Table 1), being 41–33 Ma in eastern Tibet (Chung *et al*. 1998; Wang *et al*. 2001, 2002), 36–33 Ma in the Lanping-Simao area (Zhu *et al*. 2009; Lu *et al*. 2012), 27–24 Ma in northern Laos (Nagy *et al*. 2000) and 16–0 Ma in southern Vietnam (Lee *et al*. 1998; An *et al*. 2017). In addition, these rocks can be sub-divided into an early phase from ca. 40 to 30 Ma (*e.g*. Chung *et al*. 1998; Wang *et al*. 2001, 2002; Lu *et al*. 2012) and a late phase from ca. 24 to 0 Ma (*e.g*. Akciz *et al*. 2008; Turner *et al*. 1993, 1996; Chung *et al*. 1998; Nagy *et al*. 2000; Song *et al*. 2010).

The mechanism of magma generation for these rocks is also debated, and the following models have been proposed: (1) eastward continental under-thrusting of India, leading to fluid infiltration into the overlying mantle wedge and subsequent melting (Wang *et al*. 2001); (2) movement along the Ailaoshan–Red River Shear Zone and resultant tectonic decompression (Leloup *et al*. 1995, 1999; Nagy *et al*. 2000; Liang *et al*. 2006, 2007);

CONTACT Xin Yao yaoxinphd@163.com Key laboratory of Neotectonic Movement and GeoHazard, Ministry of Land and Resources, Institute of Geomechanics, Chinese Academy of Geological Sciences, Beijing 100081, China
Supplemental data for this article can be accessed here

© 2018 Informa UK Limited, trading as Taylor & Francis Group

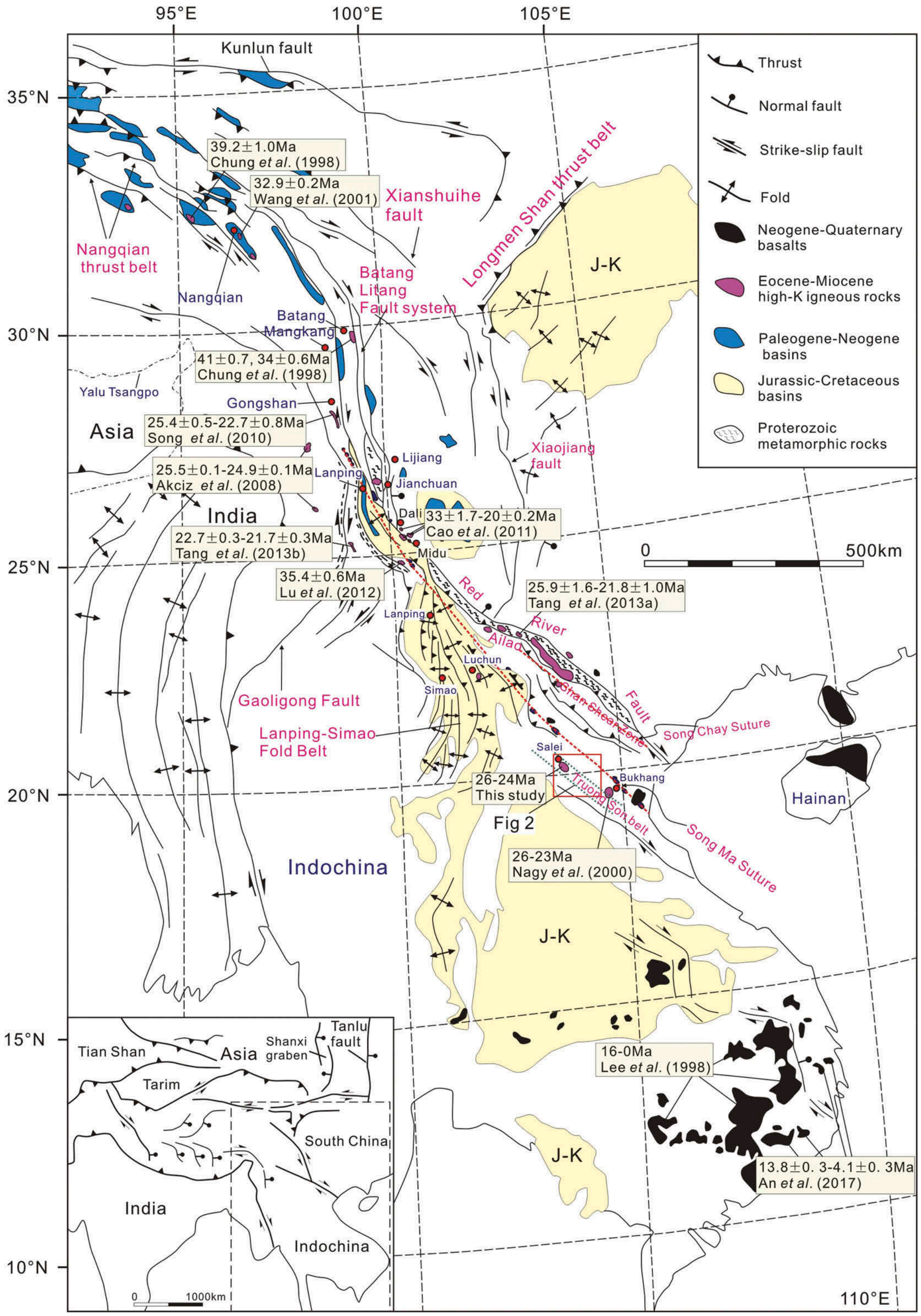

Figure 1. Cenozoic tectonic map of eastern Tibet and Indochina (modified after Wang *et al.* 2001).

and (3) convective removal of thickened lower continental lithospheric mantle (Chung *et al.* 1998; Lu *et al.* 2013).

Previous studies have provided critical information on the tectonic evolution of the eastern Tibet Plateau, as well as Lanping-Simao area; however, there is a limited understanding of the late Oligocene to early Miocene igneous rocks of the Lanping-Simao area and the Indochina Block. Although the ages of these rocks have been studied in detail (Akciz *et al.* 2008; Nagy *et al.* 2000; Song *et al.* 2010; Cao *et al.* 2011; Tang *et al.* 2013a, 2013b), their petrogenesis and magmatic evolution remain uncertain because of a lack of geochemical data.

Table 1. Summary of sample localities, lithology, and ages of the Late Oligocene to Early Miocene potassic magmatism in Eastern Tibet and Indochina block.

Sample	Location	Lithology	Age(Ma)	± 2σ	Method	Reference
Lanping-Simao area						
98JL18.4	NW of Lanping	Leucogranite	25.53	0.08	Monazite U–Pb	Akciz *et al.* (2008)
98JU27.1	SW of Lanping	Leucogranite	24.92	0.1	Monazite U–Pb	Akciz *et al.* (2008)
DC0822–1	NW of Midu	Granite	26.95	0.34	Zircon U-Pb LA-ICPMS	Cao *et al.* (2011)
DC0835-1	NW of Midu	Granite	25.31	0.18	Zircon U-Pb LA-ICPMS	Cao *et al.* (2011)
DC08-2-1	NW of Midu	Granitic Pegmatite	25.49	0.41	Zircon U-Pb LA-ICPMS	Cao *et al.* (2011)
DC08-8–5	NW of Midu	Granitic Pegmatite	22.91	0.19	Zircon U-Pb LA-ICPMS	Cao *et al.* (2011)
DC0810-2	NW of Midu	Granitic Pegmatite	20.27	0.23	Zircon U-Pb LA-ICPMS	Cao *et al.* (2011)
NJ66	SE of Gongshan	Leucogranite	22.7	0.8	Zircon U-Pb LA-ICPMS	Song *et al.* (2010)
ST122	SE of Gongshan	Tourmaline granite	24.4	0.7	Zircon U-Pb LA-ICPMS	Song *et al.* (2010)
NJ74	SE of Gongshan	Tourmaline granite	25.4	0.5	Zircon U-Pb LA-ICPMS	Song *et al.* (2010)
AL0841-8	SE of Honghe	Biotite plagioclase granitoids	21.8	1	Zircon U-Pb LA-ICPMS	Tang *et al.* (2013a)
AL0814-2	SE of Honghe	Granitic rocks	25.9	1.6	Zircon U-Pb LA-ICPMS	Tang *et al.* (2013a)
10GLG01-2	West of Yongping	Tourmaline granite	21.7	0.3	Zircon U-Pb LA-ICPMS	Tang *et al.* (2013b)
10GLG05-1	West of Yongping	Tourmaline granite	22.7	0.3	Zircon U-Pb LA-ICPMS	Tang *et al.* (2013b)
The potassic granitoids in Indochina blocks						
LS3	Xiengkhouang Plateau (Northern Laos)	Syenogranite	24	0.6	Zircon U-Pb LA-ICPMS	This study
LS4	Xiengkhouang Plateau	Syenogranite	26	0.7	Zircon U-Pb LA-ICPMS	This study
LS5	Xiengkhouang Plateau	Syenogranite	27	0.3	Zircon U-Pb LA-ICPMS	This study
LS6	Xiengkhouang Plateau	Syenogranite	24	0.4	Zircon U-Pb LA-ICPMS	This study
LS8	Xiengkhouang Plateau	Syenogranite	25	0.6	Zircon U-Pb LA-ICPMS	This study
LS9	Xiengkhouang Plateau	Syenogranite	27	0.4	Zircon U-Pb LA-ICPMS	This study
VGS-32	The northern Bu Khang (Central Vietnam)	Ganonite	26	0.2	LA-ICPMS	Nagy *et al.* (2000)
VGS-33	The northern Bu Khang	Granite	23.7	______	LA-ICPMS	Nagy *et al.* (2000)

This contribution presents new geochronological, geochemical, and Sr–Nd–Hf isotopic data from A-type granites in Laos, with the aims of (1) understanding the magma source regions of the late Oligocene granitoids and their petrogenesis; (2) constraining the emplacement ages of the granites; and (3) gaining insights into the mechanism that led to their generation.

2. Geological setting and sampling

Samples were collected from the Salei granite pluton, which is located at the northeastern edge of the Xiengkhouang Plateau, at an average elevation of 2000 m a.s.l. (Figure 2). The Salei pluton is located ~ 100 km northwest of the Bu Khang Dome, which was active from 32 to 22 Ma (Jolivet *et al.* 1999; Nagy *et al.* 2000; Figure 2), and is situated within the Truong Son Belt of the Song Ma Suture Zone. The Song Ma Suture Zone (Figure 1) consists of the Song Ca volcanic arc, the Truong Son Belt (Truong Son arc granitoids) and the Song Ma tectonic mélange, from west to east. The Song Ca volcanic arc is composed mainly of calc-alkaline volcanics, with ages of 270 to 248 Ma obtained by $^{40}Ar/^{39}Ar$ dating (Lan *et al.* 2003). The Truong Son Belt consists of widespread late Paleozoic to early Mesozoic intrusions (Liu *et al.* 2012; Wang *et al.* 2016). The stratigraphy of the Truong Son Belt includes Neoproterozoic high-grade metamorphic rocks; Silurian to Lower Devonian and upper Permian marine sedimentary rocks; upper Permian basalt, amygdaloidal basalt, and tuffs; and Triassic marine and terrigenous sedimentary rocks (DGMV 2005). The Song Ma mélange is defined as the boundary between the Indochina and South China blocks, and it formed during the westward subduction of the South China Sea under the Indochina Block in the late Permian to Early Triassic (*e.g.* Lepvrier *et al.* 2004, 2008; Liu *et al.* 2012; Faure *et al.* 2014; Wang *et al.* 2016; Figure 1). The mélange consists of sheets of Neoproterozoic to early Triassic rocks that are highly sheared, juxtaposed along shear zones, and intruded by gabbro, plagiogranite, granodiorite, and granite (DGMV 2005). East of the Song Ma mélange are tectonic units of the South China Block (Lepvrier *et al.* 2004; 2008; Faure *et al.* 2014; Wang *et al.* 2016; Figure 1) including Proterozoic greenschist to amphibolite facies metamorphic rocks of the Nam Co Complex, marine carbonates, mafic to ultramafic volcanic rocks and continental facies sediments of the Song Da Rift Zone, Mesozoic continental sediments of the Tu Le Basin, and the Song Chay Suture Zone, which was cut by the Ailaoshan-Red River shear zone in the Cenozoic.

The Salei granite pluton intruded Triassic purple sandstone and silt that are monoclinal and dip to the northeast. Samples LS-3, −4, −5, −6, −8 and −9 were collected from different parts of the Salei pluton. The contact between these strata and the Salei pluton is hidden by soil and vegetation.

3. Analytical method

Six granite samples were prepared for zircon U-Pb LA-ICP-MS dating. Zircons were separated using conventional heavy-liquid and magnetic techniques. Pure zircon

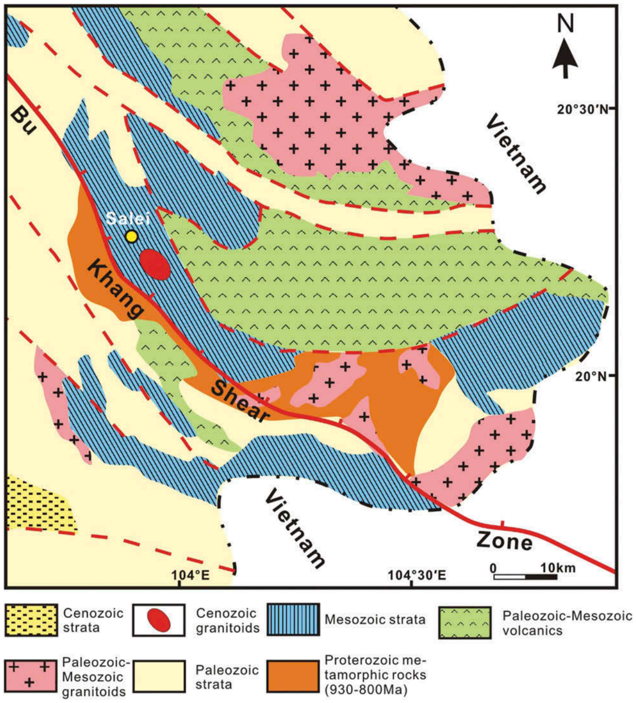

Figure 2. Geological map of the Salei pluton (modified after DGMV 2005). Yellow star indicates the location of the Salei granite pluton. The age of Proterozoic metamorphic rocks is from Nagy *et al*. (2000).

grains were selected using a binocular microscope. Representative grains were placed into an epoxy resin, along with several standard transmission electron microscopy (TEM) samples, and ground down by about half to expose the zircon interior, before performing U-Pb dating. Before and after the dating, the transmitted and reflected light were analysed, using a microscope and backscattering images together with cathode luminescence images, to determine the crystal shape, inner structure and dating position.

U–Pb dating on zircons was conducted using a New Wave UP193FX Excimer laser coupled with an Agilent 7500a ICPMS at the Key Laboratory of Continental Collision and Plateau Uplift, Institute of Tibetan Plateau Research, Chinese Academy of Sciences, Beijing. The diameter of the laser beam was 35 μm, and the duration of ablation was 45 s. The standard zircon 91,500 was used as an external standard to correct the isotopic ratios, the TEM zircon was used as a monitor and the concentrations of the elements were calculated using NIST612 glass as the external standard and ^{29}Si as the internal standard. The age data were processed using Glitter 4.4 software (details can be found in Jackson *et al*. (2004)), and the diagrams were produced using the Isoplot 3.0 Toolkit (Ludwig 2003).

In-situ Hf isotope analysis was done on zircon grains using LA-ICP-MS with a beam size of 60 μm and laser pulse frequency of 8 Hz. Details of instrument conditions and data acquisition were given in Wu *et al*. (2006) and Xie *et al*. (2008). During the analysis, $^{176}Hf/^{177}Hf$ ratios of the zircon standard (91,500) were 0.282286 ± 12 (2σ, n = 21). The $\varepsilon_{Hf}(t)$ values (parts in 104 deviation of initial Hf isotope ratios between the zircon sample and the chondritic reservoir) and T_{DM2} (zircon Hf isotope crustal model ages) based on a depleted-mantle source and an assumption that the protolith of the zircon's host magma has the average continental (crustal $^{176}Lu/^{177}Hf$ ratio of 0.015) were calculated following Griffin *et al*. (2002), using the ^{176}Lu decay constant given in Blichert-Toft and Albarède (1997). About six granite samples were chosen for whole-rock major, rare earth and trace elements analysis. Samples for elemental analysis were powdered to < 20 μm using an agate mill. Major elements analyses were conducted at the Institute of Geology and Geophysics, CAS. Major element abundances (wt.%) were determined on whole-rock samples by a Phillips PW X-ray fluorescence spectrometer (XFR-2400) and yielded analytical uncertainty < 5% (± 1σ). Rare earth and other trace elements were analysed using ICP-MS techniques at the Institute of Tibetan Plateau Research, CAS. The detailed operating conditions for the laser ablation system, the ICP-MS instrument and data reduction were the same as those described by Liu *et al*. (2008), with the uncertainties for all elements less than 5%.

Sr and Nd isotopic measurements were performed on a Nu Plasma II multi-collector inductively coupled plasma mass spectrometer (MC-ICP-MS□Nu Instruments Ltd., UK) at LCPU (Laboratory of Continental Collision and Plateau Uplift), ITP CAS (Institute of Tibetan Plateau Research, Chinese Academy of Sciences). All measured Sr and Nd ratios are fractionation corrected to $^{86}Sr/^{88}Sr = 0.1194$ and $^{146}Nd/^{144}Nd = 0.7219$, respectively. The $^{87}Sr/^{86}Sr$ ratio of the NBS987 Sr standard was 0.710248 ± 4 (2σ), and the $^{143}Nd/^{144}Nd$ ratios of the JNDI-1 Nd standard solutions were 0.512113 ± 10(2σ). For the calculation of I_{Sr}, $\varepsilon_{Nd}(t)$ and Nd model ages, the following parameters were used: $\lambda Rb = 1.42 \times 10^{-11}$ year^{-1} (Steiger and Jäger 1977); $\lambda Sm = 6.54 \times 10^{-12}$ year^{-1} (Lugmair and Marti 1978); $(^{147}Sm/^{144}Nd)_{CHUR} = 0.1967$, $(^{143}Nd/^{144}Nd)_{CHUR} = 0.512638$ (Jacobsen and Wasserburg 1980); $(^{143}Nd/^{144}Nd)_{DM} = 0.513151$, $(^{147}Sm/^{144}Nd)_{DM} = 0.2136$ (Liew and Hofmann 1988).

4. Analytical results

4.1. U–Pb zircon geochronology and in situ Lu–Hf isotopic analysis of the salei pluton

Six granite samples were prepared for U–Pb zircon dating by LA–ICP–MS; the analytical methods are outlined in Section 3, with results provided in Figure 2 and

Supplementary Table 1 (errors are all at 1σ). Zircons from samples LS-3, −4, −5, −6, −8 and −9 are light yellow to transparent, euhedral and prismatic. Cathodoluminescence images (CL) show that these zircons generally have luminescent (low-U) cores that show euhedral fine-scale oscillatory igneous zoning. They generally range from 120 to 200 μm in length and 50 to 80 μm in width. We selected 25–35 representative zircons from samples LS-3, −4, −5, −6, −8 and −9 for U–Pb dating (Supplementary Table 1). The mean Th/U ratios are 0.43, 0.39, 0.56, 0.58, 0.46 and 0.52, respectively, indicating a magmatic origin. The analyses generally group together and yield weighted mean $^{206}Pb/^{238}U$ ages of 24 ± 0.6 Ma for LS-3 (MSWD = 1.0, 1σ), 26 ± 0.7 Ma for LS-4 (MSWD = 1.8, 1σ), 26 ± 0.3 Ma for LS-5 (MSWD = 1.6, 1σ), 26 ± 0.4 Ma for LS-6 (MSWD = 0.8, 1σ), 26 ± 0.3 Ma for LS-8 (MSWD = 1.5, 1σ) and 26 ± 0.4 Ma for LS-9 (MSWD = 1.1, 1σ) (Figure 3). We interpret these ages to represent the timing of crystallization of these samples and the Salei pluton as a whole.

We selected samples LS-3, −4, −8 and −9 for *in situ* Lu–Hf isotopic analyses on zircon, based on the results of the U–Pb dating. Around 20 spots were analysed from each sample; the analytical methods are defined in Section 3, and results are provided in Figure 4 and Supplementary Table 2 (errors are all at 1σ). All zircons from samples LS-3, −4, −8 and −9 are of magmatic origin. The samples lack inherited zircons and U–Pb ages ranging from 26 to 24 Ma. These four samples have $^{176}Hf/^{177}Hf$ ratios of 0.282198–0.282764, 0.282576–0.282750, 0.282602–0.282841 and 0.282509–0.282731, respectively. The majority of spot analyses yielded negative $\varepsilon_{Hf}(t)$ values; however, some are positive. The mean $\varepsilon_{Hf}(t)$ values for these four samples are −4.3, − 3.2, −1.9 and −2.8, respectively. The mean crustal Hf two-stage model ages (T_{DM2}) are 1.38, 1.31, 1.23 and 1.29 Ga, respectively (Figure 4).

4.2. Whole-rock major, trace and rare earth element geochemistry

Major, trace and rare earth element geochemical data for the six granitic rocks sampled from the Salei pluton are listed in Supplementary Table 3, and the analytical methods are described in Section 3. The LS series granitic samples yield a narrow range of compositions, with SiO_2 of 74. 6to 77.5 wt.% and $Na_2O + K_2O$ of 8.1 to 8.4 wt.%. The K_2O contents are much higher than Na_2O contents in these rocks, with K_2O/Na_2O ranging from 1.2 to 1.4. On the Q–A–P diagram (Figure 5(a)), all samples plot within the syenogranite field. On the SiO_2–K_2O+ Na_2O diagram of Middlemost (1994), all samples fall within the granite field (Figure 5(b)). The SiO_2–K_2O diagram (Peccerillo and Taylor 1976) shows that all the granitic rocks are high-K calc-alkaline (Figure 5(c)). Their Al_2O_3 contents range from

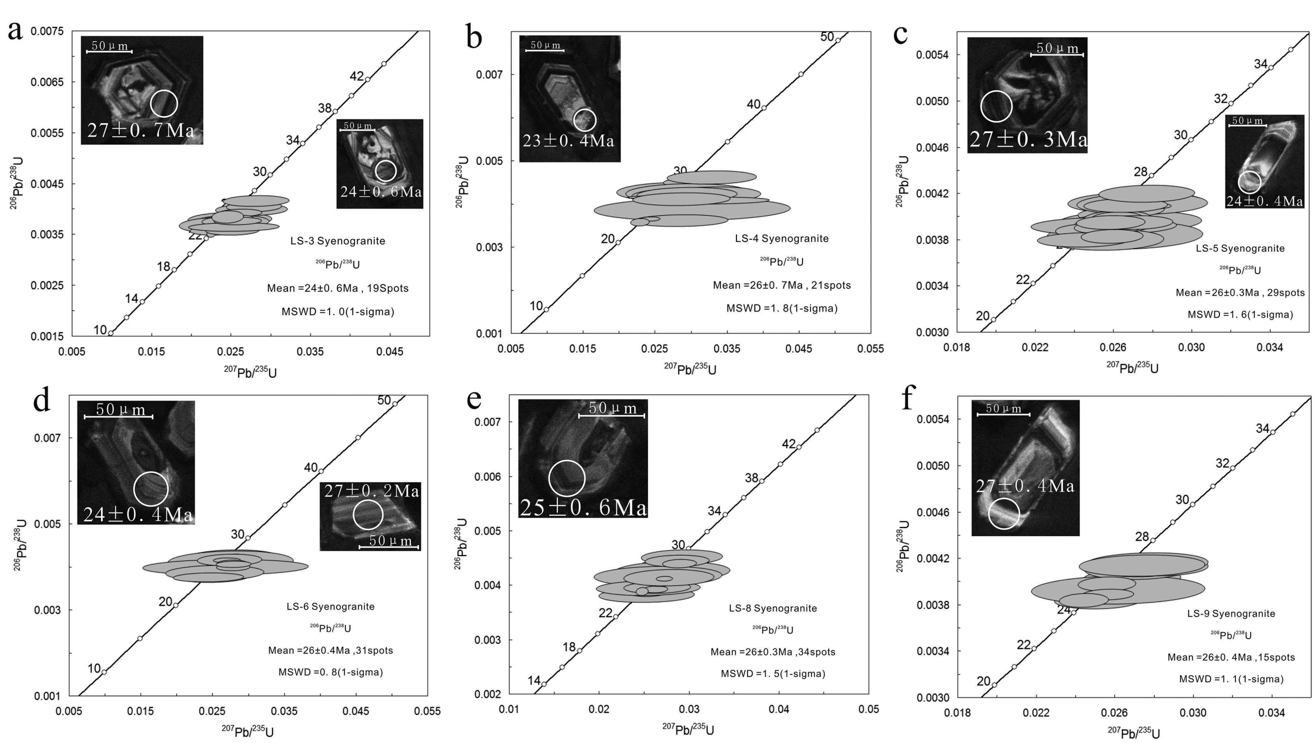

Figure 3. Cathodoluminescence (CL) images of representative zircon grains and zircon age concordia diagrams of the Salei granites in northern Laos.

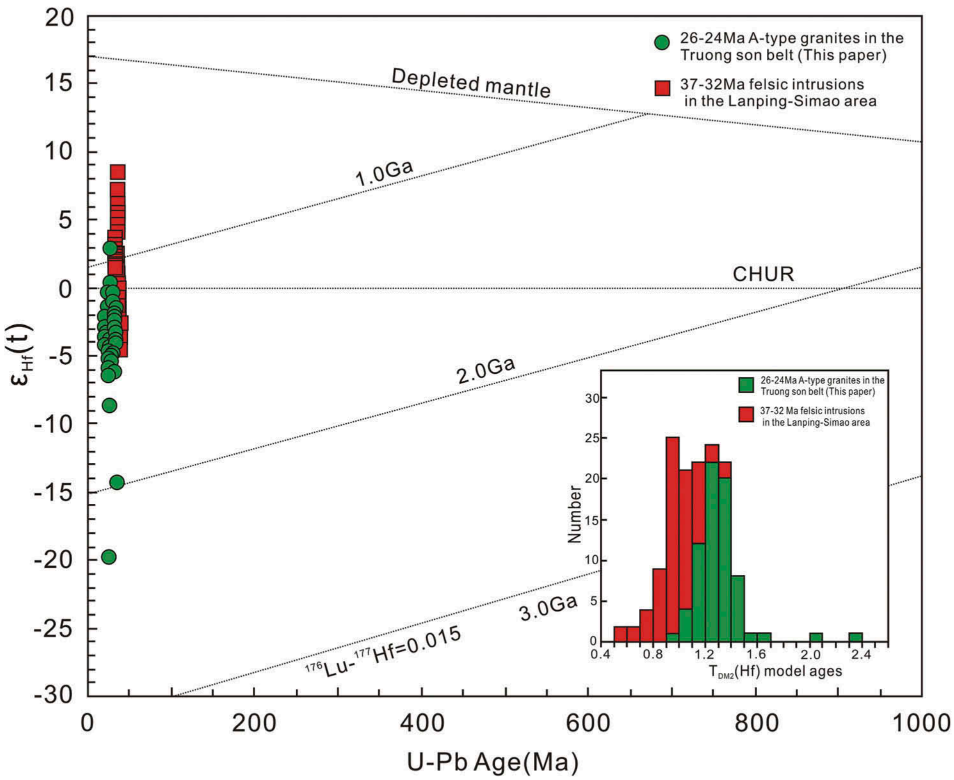

Figure 4. ε_{Hf}(t) vs. U–Pb age diagram for the Salei granites in northern Laos. Data points for 37–32 Ma felsic intrusions (Lu *et al.* 2012) from the Lanping–Simao area are shown for comparison.

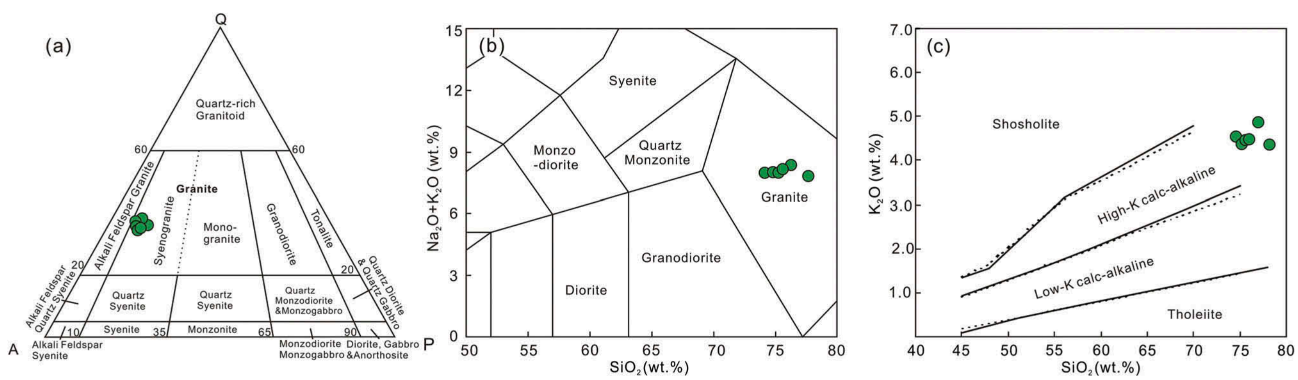

Figure 5. (a) Quartz–alkali feldspar–plagioclase (QAP) diagram (after Streckeisen 1976) for the Salei granites. (b) (K_2O + Na_2O) vs. SiO_2 classification diagram (after Middlemost 1994) for the Salei granites. (c) K_2O vs. SiO_2 diagram (after Peccerillo and Taylor 1976) showing the calc-alkaline to high-K calc-alkaline character of the Salei granites.

12.5 to 12.8 wt.%, aluminium saturation index (A/CNK) values range from 1.00 to 1.04, and Litam index values range from 1.9 to 2.0(< 3.3); thus, the samples are peraluminous high-K calc-alkaline granites.

Samples LS-3, −4, −5, −6, −8 and −9 show similar patterns on chondrite-normalized (Boynton 1984) and N-MORB-normalized (N-MORB = Normal Mid-Ocean ridge basalt; Sun and McDonough 1989) rare earth and trace element plots. The rocks show light rare earth element (LREE) enrichment and flat heavy rare earth element (HREE) patterns on a chondrite-normalized rare earth element (REE) diagram (Figure 6(a)). The value of LREE/HREE ranges from 3.4 to 7.4, and La_N/Yb_N ranges from 3.2 to 6.6. A negative Eu anomaly is observed with a mean δEu value of ~ 0.18. The rocks show variable enrichments in Rb, Th and U, and depletions in Ba, Sr, Ti and Nb (Figure 6(b)).

4.3. Sr–Nd isotopes

Sr and Nd isotopic compositions of the Salei pluton are listed in Supplementary Table 4. Six samples of the pluton

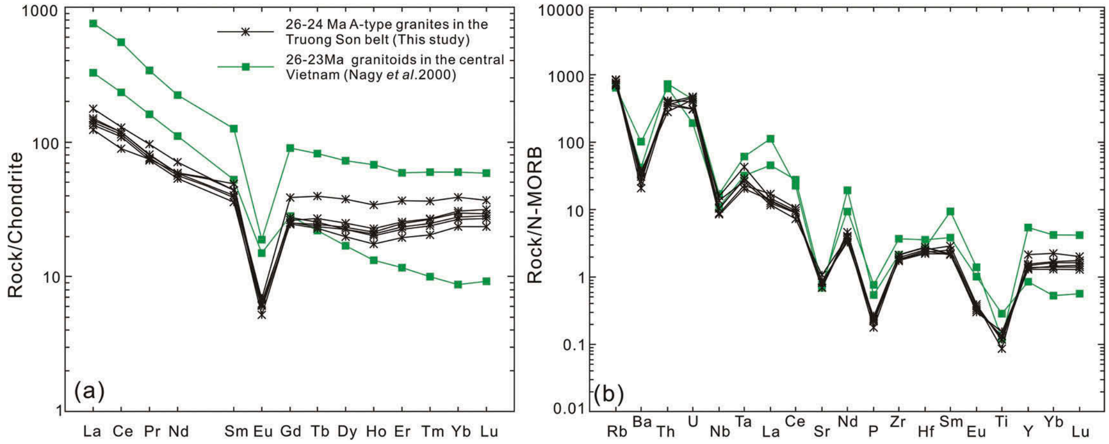

Figure 6. (a) Chondrite-normalized REE diagram (Boynton 1984) and (b) primitive-mantle-normalized trace earth diagram (Sun and McDonough 1989) for the Salei granites of northern Laos.

were selected for Sr–Nd isotopic analysis. They exhibit high $^{87}Sr/^{86}Sr$ ratios (0.741734–0.746650) and consistent $^{143}Nd/^{144}Nd$ ratios (0.512035–0.512062) (Supplementary Table 4). Initial $^{87}Sr/^{86}Sr$ ratios vary from 0.734291 to 0.741200, and $\varepsilon_{Nd}(t)$ values range from -11.6 to -11.1. The samples yield a narrow range of T_{DM2}(Nd) model ages (1737–1764 Ma), slightly higher than their T_{DM2}(Hf) model ages (1.29–1.38 Ga) (Supplementary Table 2).

5. Discussion

5.1. Tectonic setting

Granitoids have traditionally been grouped into I-, S-, M-, and A-types (Chappell and White 1974; Loiselle and Wones 1979). Accordingly, they provide petrogenetic 'Windows' into the evolution of deeper crustal sources. Moreover, different granitoids usually represent different tectonic settings during the evolution of orogency, including subduction, syn- to post-collisional and post-orogenic extensional settings (*e.g.* Chappell and White 1974, 1992; Brown 1994; Barbarin 1999; Bonin 2007). For example, many peralkaline and alkaline granites are associated with post-tectonic within-plate extension (e.g. Bonin 2007), whereas subduction-related granites tend to be metaluminous, although some metaluminous granites are collision-related (e.g. Martin 1987; Wedepohl 1991). In addition, granites related to continent–continent collision tend to be peraluminous (Wedepohl 1991; Chappell and White 1992). However, several studies have demonstrated that the majority of collision-related, strongly peraluminous granites were emplaced in post-collisional settings after the peak of crustal thickening (Sylvester 1998). The original definition of the term A-type focused on anhydrous granites with low oxygen fugacity originating from alkali basaltic magmas, and the other form of A-type granite is derived from melting of the dehydrated lower crust (Loiselle and Wones 1979). During subsequent studies (Collins *et al*. 1982; Whalen *et al*. 1987; Eby 1990, 1992; Creaser *et al*. 1991; Frost and Frost 1997; Bonin 2007), the term has been applied to a much broader spectrum of granites. The geochemical characteristics of these granites include relatively high SiO_2, K_2O, total alkalis ($Na_2O + K_2O$), ($Na_2O + K_2O$)/CaO, FeO^T/MgO, Ga/Al, and high field strength elements (HFSE; Zr, Y, Nb, Ce), low Al_2O_3 and CaO contents, and low concentrations of those trace elements compatible in mafic silicates (Cr, Ni, Co, and Sc) and feldspars (Ba, Sr, and Eu). The samples of the present study display most of the geochemical characteristics of A-type granites, including high SiO_2 (74.57–76.05 wt.%), $K_2O + Na_2O$ (8.06–8.37 wt.%), $FeO^T/(FeO^T + MgO)$ (0.93–0.97), Nb (20–37 ppm), and 10,000 × Ga/Al (1.41–1.56). Discrimination diagrams have been widely applied to distinguish A-type granites from the other granite types (Whalen *et al*. 1987; Eby 1990, 1992). On the K_2O/MgO and FeO^T/MgO vs. 10,000 × Ga/Al diagrams (Figure 7(a, b)), the studied granites plot within the A-type granite fields. The high $FeO^T/(FeO^T + MgO)$ ratio (0.93–0.97) is chemically similar to the ferroan granitoids proposed by Frost *et al*. (2001) (Figure 7(c)). On the ($Na_2O + K_2O - CaO$) vs. SiO_2 diagram (Figure 7(d)), the studied granites are alkali-calcic, plotting into the overlapping field between A- and S-type granites. Moreover, the REE patterns and trace elements are similar to the Ca. 26 Ma A-type granite in Bu Khang Dome (Figure 6 (a, b)).

The A-type granites are generally considered to be derived from relatively anhydrous, high-temperature magmas (Clemens *et al*. 1986). Based on the absence of older inherited zircons, it is inferred that the Salei granites had a high initial magmatic temperature. Zircon saturation temperatures have been calculated for the most felsic, fractionated rocks to help understand their

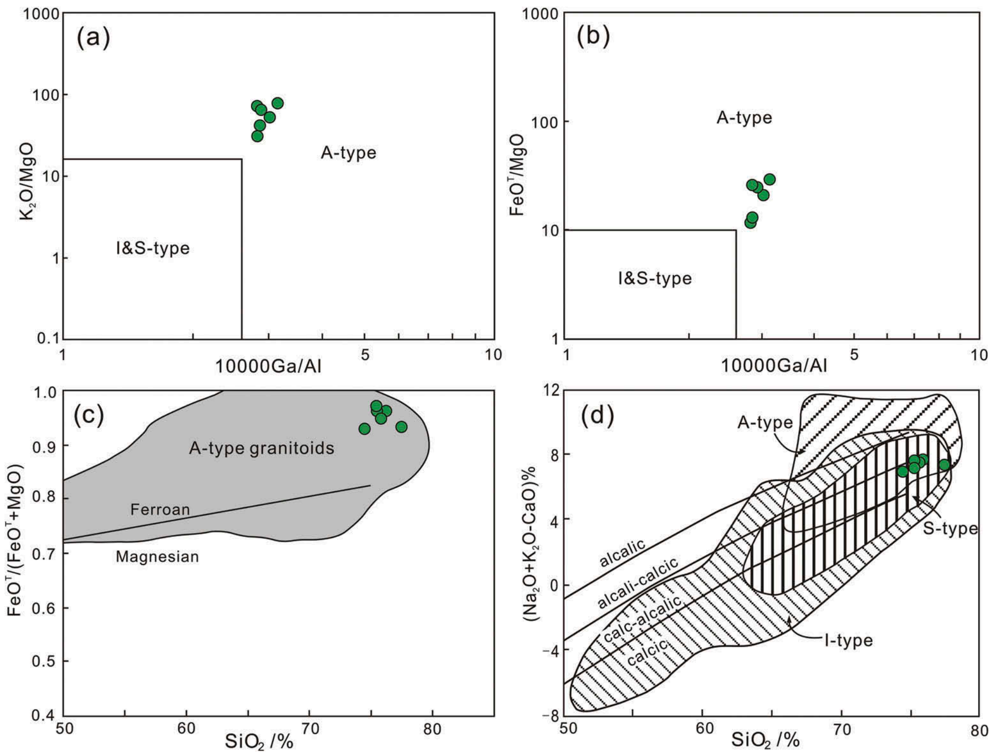

Figure 7. Discrimination diagrams for A-, I-, and S-type granites showing data of the Salei granites. (a) K_2O/MgO vs. 10,000Ga/Al diagram; (b) FeO^T/MgO vs. 10,000Ga/Al diagram; (c) $FeO^T/(FeO^T + MgO)$ vs. SiO_2 diagram; and (d) $(Na_2O + K_2O - CaO)$ vs. SiO_2 diagram. (a) and (b) are after Whalen *et al*. (1987); (c) and (d) are after Frost *et al*. (2001).

petrogenesis (Watson 1979; Watson and Harrison 1983). The calculated temperatures are between 770°C and 785°C (Supplementary Table 3, the M values are range from 1.34 to 1.41), lower than the average temperature of A-type granites. As granites undergo fractional crystallization, Zr contents generally decrease. This occurs because the melt becomes more felsic and the temperature falls, resulting in decreased Zr solubility and precipitation, and the overall removal of zircon (Watson 1979). Therefore, the relatively low zircon saturation temperatures and high SiO_2 contents of these samples are consistent with the hypothesis that zircon was precipitating and being removed from the evolving melts.

Previous studies have sub-divided the A-type granites into peralkaline A-type and aluminous A-type, there should be a pronounced difference in the geochemical compositions of these two A-types. The aluminous A-type granites typically have higher Al_2O_3 contents (> 12%) and A/CNK values (> 0.95) than peralkaline A-type granites (Qiu *et al*. 2000). The Salei granites have relatively high Al_2O_3 contents (12.5–12.8 wt. %) and A/CNK values (1.00–1.04), indicating that they are typical aluminous A-type granites.

Although A-type granites can be found in various continental and oceanic environments, in terms of tectonics they form mainly in extensional within-plate settings (*e.g*. continental rifts and oceanic islands) and post-collisional orogenic zones (Bonin 2007). According to Eby's (1990, 1992) statistical study on A-type granites worldwide, there is no clear boundary between within-plate A1-type and post-collisional A2-type granites, which exist along a continuous spectrum termed 'anorogenic granites'. Despite this, A-type granites, including post-collisional A2-type, within-plate A1-type, and anorogenic granites that correspond to neither A1- or A2-type, always represent continent–continent post-collisional orogenic processes, and their occurrence implies either an anorogenic or non-compressive setting at the end of an orogenic cycle (Dargahi *et al*. 2010). On the Nb–Y–3Ga and Ce/Nb versus Y/Nb discrimination diagrams (Figure 8(a, b)), data for the Salei granites are plotted in the A2-type field. In addition, data for these granites plot in the post-collisional and within-plate granite fields on the tectonic discrimination diagrams of Pearce *et al*. (1984) (Figure 9(a, b)), indicating a post-collisional or within-plate setting during their formation.

Whole-rock major elements show that the samples are peraluminous high-K calc-alkaline granite, and the rare earth and trace element patterns are typical of A-type within-plate granites. The geochemical characteristics of the Salei pluton are similar to the A-type

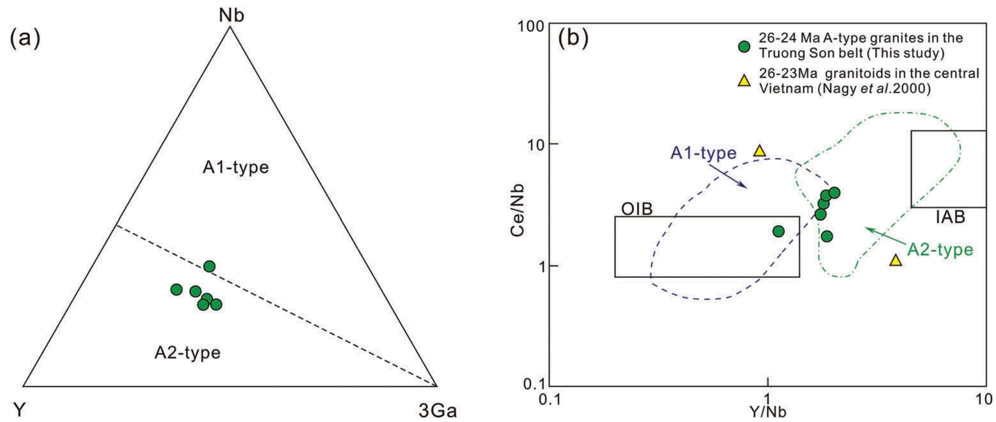

Figure 8. (a) Nb–Y–3Ga and (b) Ce/Nb vs. Y/Nb diagrams for discriminating A1- and A2-type granites, showing data of the Salei granites (after Eby 1992). The A1-type represents within-plate granites, while the A2-type represents post-collision granites.

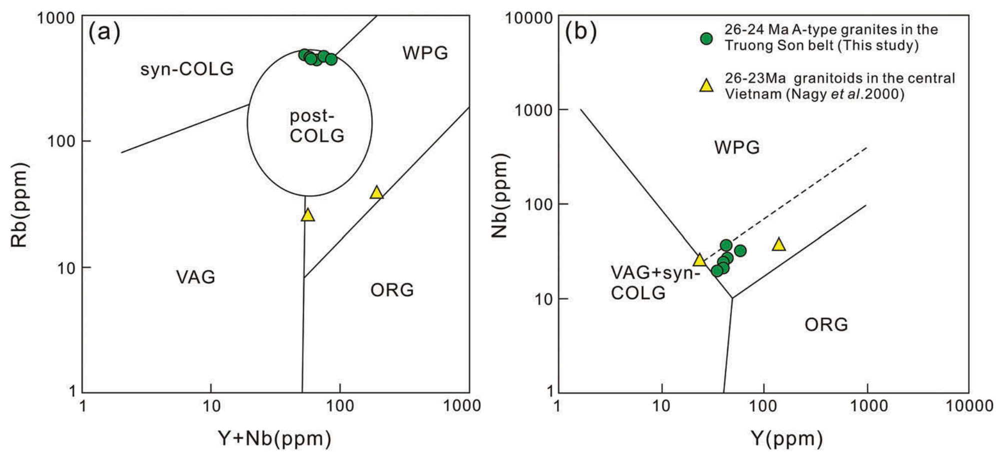

Figure 9. Tectonic discrimination diagrams for the Salei granites. VAG (volcanic-arc granites), ORG (ocean-ridge granites), WPG (within-plate granites), syn-COLG (syn-collision granites) (after Pearce *et al*. 1984; Pearce 1996).

granite of the Bu Khang Dome (26–24 Ma; Nagy *et al*. 2000), located 100 km southeast of the Salei pluton also within the Truong Son Belt. The A-type granites of the Bu Khang Dome also indicate that the Indochina Block has experienced intraplate extension since 26 Ma (Figure 9(a, b)).

5.2. Petrogenesis of the granites

As mentioned above, the Salei granites show typical A-type granite affinities. Several petrogenetic models have been proposed for the origin of A-type granites, including: (1) the partial melting or direct fractionation of mantle-derived basaltic magma (Eby 1990, 1992; Kerr and Fryer 1993; Frost and Frost 1997); (2) partial melting of felsic crust (*e.g*. Clemens *et al*. 1986; Creaser *et al*. 1991; Patiño Douce and Beard 1995; King *et al*. 1997; Patiño Douce 1997); and (3) a combination of crust-derived felsic magma and mantle-derived mafic magma (*e.g*. Foland and Allen 1991; Frost and Frost 1997; Mingram *et al*. 2000).

The Salei granites have high SiO_2 and low MgO contents, which according to Taylor and Mclennan (1995) cannot be produced directly by partial melting of mantle-derived material, as this would generate mafic and/or intermediate magmas (Hofmann 1988; Barker *et al*. 1995). The extensive fractionation of mantle-derived melts is also an unlikely scenario, as A-type granites produced in this way would be closely associated with large volumes of coeval mafic and/or intermediate igneous rocks (Turner *et al*. 1992; Litvinovsky *et al*. 2002), which is not the case for the Salei granites. In addition, the estimated temperatures for the magma are less than 850°C, which contradicts the involvement of a mantle-derived high-temperature magma during the generation of the Salei granites.

Previous studies have proposed that the dehydration melting of calc-alkaline granitoids (granodiorite) at low pressures (4 kbar) and high temperatures (950°C) in the shallow crust (depths ≤ 15 km, such as in the middle to lower crust) is a likely source of A-type granites (Skjerlie and Johnston 1993; Patiño Douce 1997). Prominent negative Sr anomalies, coupled with high LREE and flat HREE patterns [$(Gd/Yb)_N$ = 0.8–1.0] for the Salei granites (Figure 6(b)) indicate that plagioclase was present and garnet was absent in the source, arguing against the generation of these magmas in the lower crust (Patiño Douce and Beard 1995; Watkins *et al.* 2007). Considering the old basement of the Indochina Block, a purely crustal origin is also untenable for the A-type Salei granites, regardless of the nature of the middle to upper crust in the study area. The Salei granites have much younger T_{DM2}(Hf) (~ 1.4–1.2 Ga) and T_{DM2}(Nd) (~ 1.7 Ga) model ages than those of the Precambrian meta-igneous basement rocks (Lan *et al.* 2003). As such, the Proterozoic basement rocks of the Indochina Block cannot be the sole candidates for the source.

Based on the Sm–Nd isotope composition of basement rocks of the Indochina Block, there may have been a two-stage crust-forming event in the Indochina Block (Lan *et al.* 2003; Figure 10), with the first stage occurring during 2.4–1.8 Ga (Figure 10(a), solid lines) and the second during 2.1–1.2 Ga (Figure 10(a), dotted lines) (av. = 1.5 Ga, mainly 1.45–1.35 Ga; Lan *et al.* 2003). The T_{DM2}(Nd) model ages for the Salei granites are all ~ 1.7 Ga (Supplementary Table 4), while the T_{DM2}(Hf) model ages are between 1.4 and 1.2 Ga. Clearly, the protolith of the Salei granites belongs to basement rocks corresponding to the second crust-forming stage of the Indochina Block. However, on the $(^{87}Sr/^{86}Sr)_i$ versus $\varepsilon_{Nd}(t)$ diagram (Figure 10(b)), data for the Salei granites plot outside the field defined by basement rocks from the Indochina Block, indicating the addition of mantle material into the magma source of the Salei pluton. Generally, mantle material is added to a granitic magma in two ways: direct mixing between mantle-derived mafic magma and crust-derived felsic magma, or a mixed magma source derived from partial melting of both juvenile crust from an underplated mantle and ancient crust. Dark mafic enclaves are not present in the Salei pluton, and this observation, combined with the extremely low MgO contents (0.06–0.15 wt.%), indicates that the direct mixing between mantle-derived mafic magma and crust-derived felsic magma could be ruled out in the petrogenesis of these granites. Therefore, the magma source for the Salei granites was mainly the Mesoproterozoic basement rocks of the Indochina Block, mixed with a small proportion of mantle-derived juvenile crust. This view is consistent with the intrusion of mantle material into the crust during the Cenozoic (Lan *et al.* 2000).

5.3. Geodynamic implications

The Cenozoic potassic magmatic rocks from eastern Tibet and the Indochina Block can be sub-divided into an early phase from ca. 40 to 24 Ma (Chung *et al.* 1998; Wang *et al.* 2001, 2002; Lu *et al.* 2012) and a later phase from ca. 20 to 0 Ma (Turner *et al.* 1993, 1996; Chung *et al.* 1998; Nagy *et al.* 2000; Wang *et al.* 2001, 2002).

The mechanism of magma generation for the early Cenozoic potassic and ultrapotassic magmatic rocks in eastern Tibet and the Indochina Block is debated, and the following geodynamic models have been proposed: (1) Eastward continental under-thrusting of India, leading to fluid infiltration into the overlying mantle wedge and subsequent melting (Wang *et al.* 2001). (2) Movement along the Ailaoshan–Red River Shear Zone

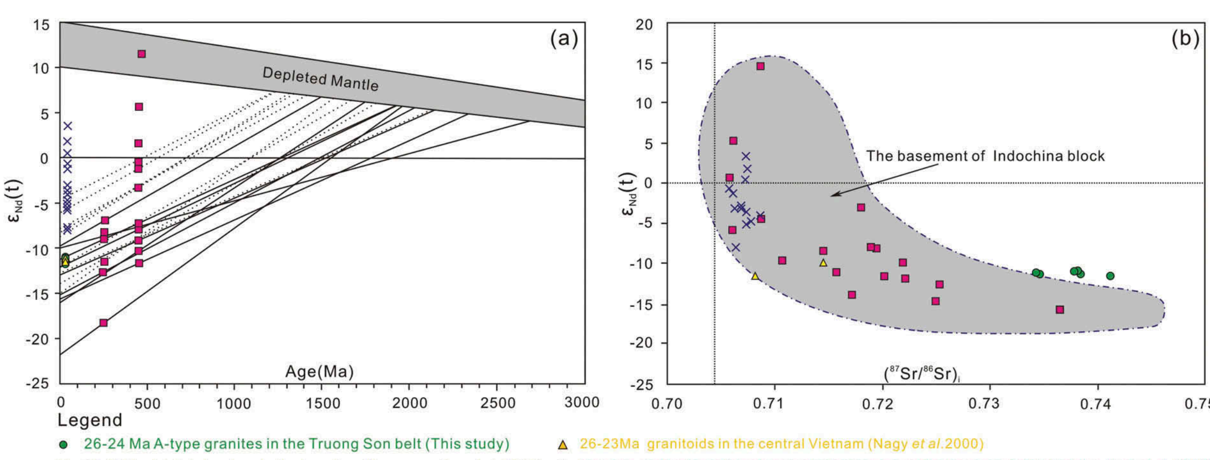

Figure 10. (a) $\varepsilon_{Nd}(t)$ vs. age diagram and (b) $\varepsilon_{Nd}(t)$ vs. $(^{87}Sr/^{86}Sr)_i$ diagram for the Salei granites. Data for 26–23 Ma granitoids of central Vietnam and 37–32 Ma felsic intrusions of the Lanping–Simao area are from Liu *et al.* (2012). The Nd isotopic evolution diagram is after Lan *et al.* (2003) and data for basement rocks of the Indochina Block are from Lan *et al.* (2003).

and resultant tectonic decompression (Leloup *et al.* 1995, 1999; Liang *et al.* 2006, 2007). (3) Convective removal of thickened lower continental lithospheric mantle (Chung *et al.* 1998; Zhao *et al.* 2009; Lu *et al.* 2013).

The eastward subduction of the Neotethyan slab under the Yangtze Craton and Indochina Block is poorly understood because of a lack of convincing geological evidence (Deng *et al.* 2013). As a result, the geodynamic model proposing the eastward continental under-thrusting of India, leading to fluid infiltration into the overlying mantle wedge, can be a high degree of uncertainty. In addition, recent extensive geochronological studies constraining the timing of ductile shearing and the emplacement of potassic–ultrapotassic rocks have shown that ductile shearing post-dates the magmatism (Lu *et al.* 2012). Therefore, it is unlikely that this shearing and continental under-thrusting generated the potassic–ultrapotassic magmatism.

The formation of widespread late Eocene to early Oligocene potassic felsic intrusions in northwestern Yunnan is ascribed to lithospheric thinning and the following asthenospheric upwelling (Lu *et al.* 2013). The dominant T_{DM2}(Hf) values of these felsic intrusions are between 1.4 and 1.0 Ga, similar to those of the A-type Salei granites (Figure 4), indicating that they may share a similar petrogenetic history. Therefore, we prefer the removal of lower lithospheric mantle as the trigger for the onset of early phase (ca. 40–24 Ma) Cenozoic potassic magmatism in eastern Tibet and the Indochina Block.

The peak T_{DM2}(Hf) model ages of granites from the Indochina Block are consistent with those of the northern Qiangtang and Changdu–Simao blocks (Wang *et al.* 2016; this study). Combined with previous work (Sengör 1979; Li *et al.* 1995, 2006; Wang *et al.* 2016, 2018), our study further confirms the concept of a single Changdu–Simao–Indochina Block. While the 26–24 Ma potassic granitoids in the Indochina block belong to the early phase (40–24) of the potassic magmatism along the eastern Tibetan plateau. However, the 26–24 Ma A-type granite indicating the extension tectonic setting in the inner section of Indochina block, contrast to the transpressional tectonics implied by the contemporaneous potassic magmtism along the eastern Tibetan plateau (Wang *et al.* 2000; Wang *et al.* 2001). In this respect, it is suggesting that the plastic deformation occurred in the inner section of the united Changdu–Simao–Indochina Block during the Late Oligocene to Early Miocene.

During the Cenozoic, the Indochina Block has been subjected to huge compressional stresses resulting from the collision between India and Eurasia, leading to thickening of the lithospheric mantle. Gravitational equilibrium then resulted in the delamination of this thickened lithospheric mantle. Asthenospheric upwelling following this delamination served as an efficient trigger mechanism for the partial melting of both juvenile and ancient crust (Figure 11). This mixed melt was then emplaced in the shallow crust and formed the A-type Salei granite.

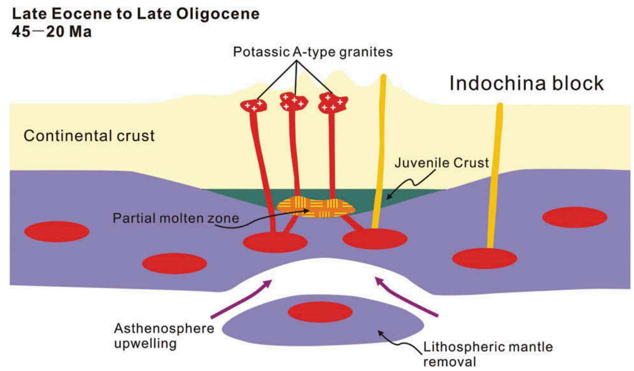

Figure 11. Schematic model of the genesis of the A-type Salei granites.

6. Conclusions

This study has allowed us to reach the following conclusions.

(1) The 26–24 Ma Salei granites in northern Laos are A-type granites and can be further classified as A2-type.
(2) Geochemical and isotopic data suggest that the A-type Salei granites were derived mainly from the partial melting of Mesoproterozoic basement rocks from the Indochina Block, along with small volumes of mantle-derived juvenile crust.
(3) The generation of the late Oligocene Salei granites is attributed to the convective removal of thickened lower continental lithospheric mantle.
(4) Formation of the A-type Salei granites in the Indochina Block corresponds to Cenozoic extension in the interior of this block.

Disclosure statement

No potential conflict of interest was reported by the authors.

Funding

This research was funded jointly by National Natural Science Foundation of China [41172192] and China Geological Survey grant No. [12120110100015001 4].

Highlights

(1) The 26-24 Ma Salei granites in the north Laos belong to the A2 sub-type of within-plate granites.
(2) The generation of the Late Oligocene Salei granites is attributed to the convective removal of thickened lower continental lithospheric mantle.
(3) The Salei A-type granites were emplaced during Cenozoic extension of the inner section of the Indochina block.

References

Akciz, S., Burchfiel, B.C., Crowley, J.L., Yin, J.Y., and Chen, L.Z., 2008, Geometry, kinematics, and regional significance of the Chong Shan shear zone, Eastern Himalayan Syntaxis, Yunnan, China: Geosphere, v. 4, p. 292–314. doi:10.1130/GES00111.1

An, A.R., Choi, S.H., Yu, Y., and Lee, D.C., 2017, Petrogenesis of Late Cenozoic basaltic rocks from southern Vietnam: Lithos, v. 272–273, p. 192–204. doi:10.1016/j.lithos.2016.12.008

Barbarin, B., 1999, A review of the relationships between granitoid types, their origins and their geodynamic environments: Lithos, v. 46, p. 605–626. doi:10.1016/S0024-4937(98)00085-1

Barker, M.B., Hirschmann, M.M., Ghiorso, M.S., and Stolper, E. M., 1995, Composition of nearsolidus peridotite melts from experiments and thermodynamic calculations: Nature, v. 375, p. 308–311. doi:10.1038/375196b0

Blichert-Toft, J., and Albarède, F., 1997, The Lu–Hf geochemistry of chondrites and the evolution of the mantle–crust system: Earth and Planetary Science Letters, v. 148, p. 243–258. doi:10.1016/S0012-821X(97)00040-X

Bonin, B., 2007, A-type granites and related rocks: Evolution of a concept, problems and prospects: Lithos, v. 97, p. 1–29. doi:10.1016/j.lithos.2006.12.007

Boynton, W.V., 1984, Cosmochemistry of the rare earth elements. Meteorite studies: Elsevier Science Publishing Company, Amsterdam

Brown, M., 1994, The generation, segregation, ascent and emplacement of granite magma: Themigmatite-to-crustally-derivedgranite connection in thickened orogens: Earth-Science Reviews, v. 36, p. 83–130. doi:10.1016/0012-8252(94)90009-4

Cao, S.Y., Liu, J.L., Leiss, B., Neubauer, F., Genser, J., and Zhao, C.Q., 2011, Oligo-Miocene shearing along the Ailao Shan–Red River shear zone: Constraints from structural analysis and zircon U–Pb geochronology of magmatic rocks in the Diancang Shan massif, SE Tibet, China: Gondwana Research, v. 19, p. 975–993. doi:10.1016/j.gr.2010.10.006

Chappell, B.W., and White, A.J.R., 1974, Two contrasting granite types: Pacific Geology, v. 8, p. 173–174

Chappell, B.W., and White, A.J.R., 1992, I- and S-type granites in Lachlan Fold Belt: Transactions of the Royal Society of Edinburgh, v. 83, p. 1–26. doi:10.1017/S0263593300007720

Chung, S.L., Lo, C.H., Lee, T.Y., Zhang, Y.Q., Xie, Y.W., Li, X.H., Wang, K.L., and Wang, P.L., 1998, Diachronous uplift of the Tibetan Plateau starting 40 Myr ago: Nature, v. 394, p. 769–773. doi:10.1038/29522

Clemens, J.D., Holloway, J.R., and White, A.J.R., 1986, Origin of an A-type granite: Experimental constraints: American Mineralogist, v. 71, p. 317–324

Collins, W.J., Beams, S.D., White, A.J.R., and Chappell, B.W., 1982, Nature and origin of A-type granites with particular reference to southeastern Australia: Contributions to Mineralogy and Petrology, v. 80, p. 189–200. doi:10.1007/BF00374895

Creaser, R.A., Price, R.C., and Wormald, R.J., 1991, A-type granites revisited: Assessment of a residual source model: Geology, v. 19, p. 163–166. doi:10.1130/0091-7613(1991)019<0163:ATGRAO>2.3.CO;2

Dargahi, S., Arvin, M., Pan, Y.M., and Babaei, A., 2010, Petrogenesis of post-collisional A-type granitoids from the Urumieh–Dokhtarmagmatic assemblage, southwestern Kerman, Iran: Constraints on the Arabian–Eurasian continental collision: Lithos, v. 115, p. 190–204. doi:10.1016/j.lithos.2009.12.002

Deng, J., Wang, Q.F., L, G.J., and Santosh, M., 2014, Cenozoic tectono-magmatic and metallogenic processes in the Sanjiang region, southwestern China: Earth-Science Reviews, v. 138, p. 268–299. doi:10.1016/j.earscirev.2014.05.015

Deng, J., Wang, Q.F., Li, G.J., Li, C.S., and Wang, C.M., 2013, Tethys tectonic evolution and its bearing on the distribution of important mineral deposits in the Sanjiang region, SW China: Gondwana Research, v. 26, p. 419–437. doi:10.1016/j.gr.2013.08.002

Department of Geological and Minerals of Vietnam (DGMV), 2005, Geology and mineral resources map of Phong Saly-Dien Bien Phu Sheet, scale 1: 200000, with the explanatory note, Hanoi.

Eby, G.N., 1990, The A-type granitoids: A review of their occurrence and chemical characteristics and speculations on their petrogenesis: Lithos, v. 26, p. 115–134. doi:10.1016/0024-4937(90)90043-Z

Eby, G.N., 1992, Chemical subdivision of the A-type granitoids: Petrogenetic and tectonic implications: Geology, v. 20, p. 641–644. doi:10.1130/0091-7613(1992)020<0641:CSOTAT>2.3.CO;2

Faure, M., Lepvrier, C., Nguyen, V., Vu, T., Lin, W., and Chen, Z., 2014, The South China block-Indochina collision: Where, when, and how?: Journal of Asian Earth Sciences, v. 79, p. 260–274. doi:10.1016/j.jseaes.2013.09.022

Foland, K.A., and Allen, J.C., 1991, Magma sources for Mesozoic anorogenic granites of the White Mountain magma series, New England, USA: Contributions to Mineralogy and Petrology, v. 109, p. 195–211. doi:10.1007/BF00306479

Frost, B.R., Barnes, C.G., Collins, W.J., Arculus, R.J., Ellis, D.J., and Frost, C.D., 2001, A geochemical classification for granitic rocks: Journal of Petrology, v. 42, p. 2033–2048. doi:10.1093/petrology/42.11.2033

Frost, C.D., and Frost, B.R., 1997, Reduced rapakivi-type granites: The tholeiite connection: Geology, v. 25, p. 647–650. doi:10.1130/0091-7613(1997)025<0647:RRTGTT>2.3.CO;2

Griffin, W.L., Wang, X., Jackson, S.E., Pearson, N.J., O'Reilly, S.Y., Xu, X., and Zhou, X., 2002, Zircon chemistry and magma-mixing, SE China: In-situ analysis of Hf isotopes, Tonglu and Pingtan igneous complexes: Lithos, v. 61, p. 237–269. doi:10.1016/S0024-4937(02)00082-8

Hofmann, A.W., 1988, Chemical differentiation of the Earth: The relationship between mantle, continental crust, and oceanic crust: Earth and Planetary Science Letters, v. 90, p. 297–314. doi:10.1016/0012-821X(88)90132-X

Jackson, S.E., Pearson, N.J., Griffin, W.L., and Belousova, E.A., 2004, The application of laser ablation-inductively coupled plasma-mass spectrometry to in situ U–Pb zircon geochronology: Chemical Geology, v. 211, p. 47–69. doi:10.1016/j.chemgeo.2004.06.017

Jacobsen, S.B., and Wasserburg, G.J., 1980, Sm-Nd isotopic evolution of chondrites: Earth and Planetary Science Letters, v. 50, p. 139–155. doi:10.1016/0012-821X(80)90125-9

Jolivet, L., Maluski, H., Beyssac, O., Goffe´, B., Lepvrier, C., Thi, P. T., and Vuong, N.V., 1999, The Oligo-Miocene Bu Khang extensional gneiss dome in North Vietnam, geodynamic implications: Geology, v. 27, p. 67–70. doi:10.1130/0091-7613(1999)027<0067:OMBKEG>2.3.CO;2

Kerr, A., and Fryer, B.J., 1993, Nd isotope evidence for crust–mantle interaction in the generation of A-type granitoid suites in Labrador, Canada: Chemical Geology, v. 104, p. 39–60. doi:10.1016/0009-2541(93)90141-5

King, P.L., White, A.J.R., Chappell, W., and Allen, C.M., 1997, Characterization and origin of aluminous A-type granites from the Lachlan Fold Belt, southeastern Australia: Journal of Petrology, v. 38, p. 371–391. doi:10.1093/petroj/38.3.371

Lan, C., Chung, S., Van Long, T., Lo, C., Lee, T., Mertzman, S., and Shen, J., 2003, Geochemical and Sr–Nd isotopic constraints from the Kontum massif, central Vietnam on the crustal evolution of the Indochina block: Precambrian Research, v. 122, p. 7–27. doi:10.1016/S0301-9268(02)00205-X

Lan, C.Y., Chung, S.L., Shen, J.J.S., Lo, C.H., Wang, P.L., Hoa, T.T., Thanh, H.H., and Mertzman, S.A., 2000, Geochemical and Sr-Nd isotopic characteristics of granitic rocks from northern Vietnam: Journal of Asian Earth Sciences, v. 18, p. 267–280. doi:10.1016/S1367-9120(99)00063-2

Lee, T.Y., Lo, C.H., Chung, S.L., Chen, C.Y., Wang, P.L., Lin, W.P., Hoang, N., Chi, C.T., and Yem, N.T., 1998, $^{40}Ar/^{39}Ar$ dating result of Neogene basalts in Vietnam and its tectonic implication, in Flower, M.F.J., Chung, S.L., and Lo, C.H., Eds., Mantle dynamics and plate interactions in East Asia, AGU geodynamic series, 27: Washington, DC, p. 317–330

Leloup, P.H., Lacassin, R., Tapponnier, P., Schärer, U., Zhong, D. L., Liu, X.H., Zhang, L.S., Ji, S.C., and Trinh, P.T., 1995, The Ailao Shan–Red River shear zone (Yunnan, China), Tertiary transform boundary of Indochina: Tectonophysics, v. 251, p. 3–84. doi:10.1016/0040-1951(95)00070-4

Leloup, P.H., Ricard, Y., Battaglia, J., and Lacassin, R., 1999, Shear heating in continental strikeslip shear zone: Numerical modelling and case studies: Geophysical Journal International, v. 136, p. 19–40. doi:10.1046/j.1365-246X.1999.00683.x

Lepvrier, C., Maluski, H., Van Tich, V., Leyreloup, A., Truong Thi, P., and Van Vuong, N., 2004, The Early Triassic Indochinan orogeny in Vietnam (Truong Son Belt and Kontum Massif); implications for the geodynamic evolution of Indochina: Tectonophysics, v. 393, p. 87–118. doi:10.1016/j.tecto.2004.07.030

Lepvrier, C., Vuong, N.V., Maluski, H., Thi, P.T., and Tich, V.V., 2008, Indosinian tectonics in Vietnam: Comptes Rendus Geoscience, v. 340, p. 94–111. doi:10.1016/j.crte.2007.10.005

Li, C., Cheng, L.R., Hu, K., Yang, Z.R., and Hong, Y.R., 1995, Study on the Paleo–Tethys suture zone of Longmu Co–Shuanghu: Tibet: Beijing, Geological Publishing House

Li, C., Huang, X.P., Zhai, Q.G., Zhu, T.X., Yu, Y.S., Zeng, Q.G., and Wang, G.H., 2006, The Longmu Co–Shuanghu–Jitang plate suture and the northern boundary of Gondwanaland in the Qinghai–Tibet Plateau, Earth Science Frontiers, v. 13(4), p. 136–147 in Chinese with English abstract

Liang, H.Y., Campbell, I.H., Allen, C., Sun, W.D., Liu, C.Q., Yu, H. X., Xie, Y.W., and Zhang, Y.Q., 2006, Zircon $Ce^{4+}/Ce+$ ratios and ages for Yulong ore-bearing porphyries in eastern Tibet: Mineralium Deposita, v. 41, p. 152–159. doi:10.1007/s00126-005-0047-1

Liang, H.Y., Campbell, I.H., Allen, C.M., Sun, W.D., Yu, H.X., Xie, Y.W., and Zhang, Y.Q., 2007, The age of the potassic alkaline igneous rocks along the Ailao Shan–Red River Shear Zone: Implications for the onset age of left-lateral shearing: Journal of Geology, v. 115, p. 231–242. doi:10.1086/510801

Liew, T.C., and Hofmann, A.W., 1988, Precambrian crustal components, plutonic associations, plate environment of the Hercynian Fold Belt of central Europe: Indications from a Nd and Sr isotopic study: Contributions to Mineralogy and Petrology, v. 98, p. 129–138. doi:10.1007/BF00402106

Litvinovsky, B.A., Jahn, B.M., Zanvilevich, A.N., Saunders, A., Poulain, S., Kuzmin, D.V., Reichow, M.K., and Titov, A.V., 2002, Petrogenesis of syenite-granite suites from the Bryansky Complex (Transbaikalia, Russia): Implications for the origin of A-type granitoid magmas: Chemical Geology, v. 189, p. 105–133. doi:10.1016/S0009-2541(02)00142-0

Liu, J., Tran, M., Tang, Y., Nguyen, Q.L., Tran, T.H., Wu, W., Chen, J., Zhang, Z., and Zhao, Z., 2012, Permo-Triassic granitoids in the northern part of the Truong Son belt, NW Vietnam: Geochronology, geochemistry and tectonic implications: Gondwana Research, v. 122, p. 628–644. doi:10.1016/j.gr.2011.10.011

Liu, Y.S., Hu, Z.C., Gao, S., Günther, D., Xu, J., Gao, C.G., and Chen, H.H., 2008, In situ analysis of major and trace elements of anhydrous minerals by LA-ICP-MS without applying an internal standard: Chemical Geology, v. 257, p. 34–43. doi:10.1016/j.chemgeo.2008.08.004

Loiselle, M.C., and Wones, D.S., 1979, Characteristics and origin of anorogenic granites: Geological Societyof America: Abstracts with Programs, v. 11, p. 468

Lu, Y.J., Kerrich, R., Cawood, P.A., McCuaig, T.C., Hart, C.J.R., Li, Z.X., Hou, Z.Q., and Bagas, L., 2012, Zircon SHRIMP U–Pb geochronology of potassic felsic intrusions in western Yunnan, SW China: Constraints on the relationship of magmatism to the Jinsha suture: Gondwana Research, v. 22, p. 737–747. doi:10.1016/j.gr.2011.11.016

Lu, Y.J., Kerrich, R., Mccuaig, T.C., Li, Z.X., Hart, C.J., Cawood, P.A., Hou, Z.Q., Bagasi, L., Cliff, J., Belousov, E.A., and Tang, S.H., 2013, Geochemical, Sr–Nd–Pb, and zircon Hf–O isotopiccompositions of Eocene–Oligocene shoshonitic and potassic adakite-like felsic intrusions in western Yunnan, SWChina: Petrogenesis and tectonic implications: Journal of Petrology, v. 54, p. 1309–1348. doi:10.1093/petrology/egt013

Ludwig, K.R., 2003, User's manual for Isoplot 3.00: A geochronological toolkit for Microsoft Excel: Berkeley Geochronology Center Special Publication, p. 4

Lugmair, G.W., and Marti, K., 1978, Lunar initial $^{143}Nd/^{144}Nd$: Differential evolution of the lunar crust and mantle: Earth and Planetary Science Letters, v. 39, p. 349–357. doi:10.1016/0012-821X(78)90021-3

Martin, H., 1987, Petrogenesis of Archean trondhjemites, tonalites and granodiorites fro eastern Finland: Major and trace element geochemistry: Journal of Petrology, v. 28, p. 921–953. doi:10.1093/petrology/28.5.921

Middlemost, E.A.K., 1994, Naming materials in the magma/igneous rock system: Earth Science Review, v. 37, p. 215–224. doi:10.1016/0012-8252(94)90029-9

Mingram, B., Trumbull, R.B., and Littman, S., 2000, A petrogenetic study of anorogenic felsic magmatism in the cretaceous paresis ring complex, Namibia: Evidence for mixing of crust and mantle-derived components: Lithos, v. 54, p. 1–22. doi:10.1016/S0024-4937(00)00033-5

Nagy, E.A., Schärer, U., and Minh, N.T., 2000, Oligocene-Miocene granitic magmatism in central Vietnam and implications for continental deformation in Indochina: Terra Nova, v. 12, p. 67–76. doi:10.1111/j.1365-3121.2000.00274.x

Patiño Douce, A.E., 1997, Generation of metaluminous A-type granites by low-pressure melting of calc-alkaline granitoids: Geology, v. 25, p. 743–746. doi:10.1130/0091-7613(1997)025<0743:GOMATG>2.3.CO;2

Patiño Douce, A.E., and Beard, J.S., 1995, Dehydration-melting of biotite gneiss and quartz amphibolite from 3 to 15 kbar: Journal of Petrology, v. 36, p. 707–738. doi:10.1093/petrology/36.3.707

Pearce, J.A., 1996, Sources and settings of granitic rocks: Episodes, v. 19, p. 120–125

Pearce, J.A., Harris, N.B.W., and Tindle, A.G., 1984, Trace element discrimination diagrams for the tectonic interpretation of granitic rocks: Journal of Petrology, v. 25, p. 956–983. doi:10.1093/petrology/25.4.956

Peccerillo, A., and Taylor, S.R., 1976, Geochemistry of Eocene calc-alkaline volcanic rocks from the Kastamonu area, northern Turkey: Contributions to Mineralogy and Petrology, v. 58, p. 63–81. doi:10.1007/BF00384745

Qiu, J.S., Wang, D.Z., Wang, D.Z., Satoshi, K., and Brent, I.A.M., 2000, Geochemistry and petrogenesis of aluminous A-type granites in the coastal area of Fujian Province: GEOCHIMICA, v. 29, p. 313–321

Sengör, A.M.C., 1979, Mid-Mesozoic closure of Permo-Triassic Tethys and its implications: Nature, v. 279, p. 590–593. doi:10.1038/279590a0

Skjerlie, K.P., and Johnston, A.D., 1993, Vapor-absent melting at 10 kbar of a biotite- and amphibole-bearing tonalitic gneiss: Implications for the generation of A-type granites: Geology, v. 20, p. 263–266. doi:10.1130/0091-7613(1992)020<0263:VAMAKO>2.3.CO;2

Song, S.G., Niu, Y.L., Wei, C.J., Ji, J.Q., and Su, L., 2010, Metamorphism, anatexis, zircon ages and tectonic evolution of the Gongshan block in the northern Indochina continent—An eastern extension of the Lhasa Block: Lithos, v. 120, p. 327–346. doi:10.1016/j.lithos.2010.08.021

Steiger, R.H., and Jäger, E., 1977, Subcommission on geochronology: Convention on the use of decay constants in geo- and cosmochronology: Earth and Planetary Science Letters, v. 36, p. 359–362. doi:10.1016/0012-821X(77)90060-7

Streckeisen, A., 1976, To each plutonic rock its proper name: Earth-Science Reviews, v. 12, p. 1–33. doi:10.1016/0012-8252(76)90052-0

Sun, S.S., and McDonough, W.F., 1989, Chemical and isotopic systematics of oceanic basalts: Implications for mantle composition and processes, *in* Saunders, A.D., and Norry, M.J., eds, Magmatism in the ocean basins: Geological Society, London, Special Publications, Vol. 42, p. 313–345

Sylvester, P.J., 1998, Postcollisional strongly peraluminous granites: Lithos, v. 45, p. 29–44. doi:10.1016/S0024-4937(98)00024-3

Tang, Y., Liu, J.L., Tran, M.D., Song, Z.J., Wu, W.B., Zhang, Z.C., Zhao, Z.D., and Chen, W., 2013a, Timing of left-lateral shearing along the Ailao Shan–Red River shear zone: Constraints from zircon U–Pb ages from granitic rocks in the shear zone along the Ailao Shan Range, western Yunnan, China: International Journal of Earth Sciences, v. 102, p. 605–626. doi:10.1007/s00531-012-0831-y

Tang, Y., Yin, F.G., Wang, L.Q., Wang, D.B., Liao, S.Y., Sun, Z.M., and Sun, J., 2013b, Structural characterization of and geochronological constraints on sinistral strike-slip shearing along the southern segment of Chongshan shear zone, western Yunnan: Acta Petrologica Sinica, v. 29, p. 1311–1324

Taylor, S.R., and Mclennan, S.M., 1995, The continental crust: Its composition and evolution, and examination of the geochemical record preserved in sedimentary rocks: BlackwellScience Publisher, Oxford

Turner, S., Arnaud, N., Liu, J., Rogers, N., Hawkesworth, C., Harris, N., Kelley, S., Van Calsteren, P., and Deng, W., 1996, Post-collision, Shoshonitic Volcanism on the Tibetan Plateau: Implications for gonvective thinning of the lithosphere and the source of ocean island basalts: Journal of Petrology, v. 37, p. 45–71. doi:10.1093/petrology/37.1.45

Turner, S., Hawkesworth, C., Liu, J., Rogers, N., Kelley, S., and Carsteren, P., 1993, Timing of Tibetan uplift constrained analysis of volcanic rocks: Nature, v. 364, p. 50–54. doi:10.1038/364050a0

Turner, S.P., Foden, J.D., and Morrison, R.S., 1992, Derivation of some A-type magmas by fractionation of basaltic magma: An example from the Padthaway Ridge, South Australia: Lithos, v. 28, p. 151–179. doi:10.1016/0024-4937(92)90029-X

Wang, E., and Burch¢El, B.C., 1997, Interpretation of Cenozoic tectonics in the right-lateral accommodation zone between the Ailao Shan shear zone and the eastern Himalayan syntaxis: International Geology Review, v. 39, p. 191–219. doi:10.1080/00206819709465267

Wang, J.H., Yin, A., Harrison, T.M., Grove, M., Zhang, Y.Q., and Xie, G.H., 2001, A tectonic model for Cenozoic igneous activities in the eastern Indo-Asian collision zone: Earth and Planetary Science Letters, v. 188, p. 123–133. doi:10.1016/S0012-821X(01)00315-6

Wang, J.H., Yin, A., Harrison, T.M., Grove, M., Zhou, J.Y., Zhang, Y.Q., and Jie, G.H., 2002, Thermal chronology of Cenozoic two-types high potassium magmatic activity along the eastern margin of the Tibetan Plateau: Science in China (Series D), v. 32, p. 529–537

Wang, S.F., Mo, Y.S., Wang, C., and Ye, P.S., 2016, Paleotethyan evolution of the Indochina block as deduced from granites in northern Laos: Gondwana Research, v. 38, p. 183–196. doi:10.1016/j.gr.2015.11.011

Wang, X.Y., Wang, S.F., Wang, C., and Tang, W.K., 2018, Permo-Triassic arc-like granitoids along the northern Lancangjiang zone, eastern Tibet: Age, geochemistry, Sr–Nd–Hf isotopes, and tectonic implications: Lithos, v. 308–309, p. 278–293. doi:10.1016/j.lithos.2018.03.008

Watkins, J.M., Clemens, J.D., and Treloar, P.J., 2007, Archaean TTGs as sources of younger granitic magmas: Melting of sodic metatonalites at 0.6–1.2 GPa: Contributions to Mineralogy and Petrology, v. 154, p. 91–110. doi:10.1007/s00410-007-0181-0

Watson, E.B., 1979, Zircon saturation in felsic liquids: Experimental data and applications to trace element geochemistry: Contributions to Mineralogy and Petrology, v. 70, p. 407–419. doi:10.1007/BF00371047

Watson, E.B., and Harrison, T.M., 1983, Zircon saturation revisited: Temperature and composition effects in a variety of crustal magma types: Earth and Planetary Science Letters, v. 64, p. 295–304. doi:10.1016/0012-821X(83)90211-X

Wedepohl, K.H., 1991, Chemical composition and fractionation of the continental crust: Geologische Rundschau, v. 80, p. 207–223. doi:10.1007/BF01829361

Whalen, J.B., Currie, K.L., and Chappell, B.W., 1987, A-type granites: Geochemical characteristics, discrimination and petrogenesis: Contributions to Mineralogy and Petrology, v. 95, p. 407–419. doi:10.1007/BF00402202

Wu, F.Y., Yang, Y.H., Xie, L.W., Yang, J.H., and Xu, P., 2006, Hf isotopic compositions of the standard zircons and baddeleyites used in U–Pb geochronology: Chemical Geology, v. 234, p. 105–126. doi:10.1016/j.chemgeo.2006.05.003

Xie, L.W., Zhang, Y.B., Zhang, H.H., Sun, J.F., and Wu, F.Y., 2008, In situ simultaneous determination of trace elements, U–Pb and Lu–Hf isotopes in zircon and baddeleyite: Chinese Science Bulletin, v. 53, p. 1565–1573

Zhao, Z.D., Mo, X.X., Dilek, Y., Niu, Y.L., DePaolo, D.J., Robinson, P., Zhu, D.C., Sun, C.G., Dong, G.C., Zhou, S., Luo, Z.H., and Hou, Z.Q., 2009, Geochemical and Sr–Nd–Pb–O isotopic compositions of the post-collisional ultrapotassic magmatism in SW Tibet: Petrogenesis and implications for India intra-continental subduction beneath southern Tibet: Lithos, v. 113, p. 190–212. doi:10.1016/j.lithos.2009.02.004

Zhu, X.P., Mo, X.X., White, N.C., Zhang, B., Sun, M.X., Wang, S.X., Zhao, S.L., and Yang, Y., 2009, Geology and metallogenetic setting of the Habo porphyry Cu (Mo–Au) deposit, Yunnan: Acta Geologica Sinica, v. 83, p. 1915–1928 in Chinese with English abstract